Supporting Information

Flatt *et al.* 10.1073/pnas.0709128105

SI Materials and Methods

Primers for Quantitative PCR (qPCR). We used the following primer pairs: *dilp2*-F, TGA GTA TGG TGT GCG AGG; *dilp2*-R, CTC TCC ACG ATT CCT TGC; *dilp3*-F, GAA CTT TGG ACC CCG TGA A; *dilp3*-R, TGA GCA TCT GAA CCG AA CT; *dilp5*-F, CAA ACG AGG CAC CTT GGG; *dilp5*-R, AGC TAT CCA AAT CCG CCA; *4E-BP*-F, GAA GGT TGT CAT CTC GGA TCC; *4E-BP*-R, ATG AAA GCC CGC TCG TAG A; *l (2)efl*-F, AGG GAC GAT GTG ACC GTG TC; *l (2)efl*-R, CGA AGC AGA CGC GTT TAT CC; *dALS*-F, TAC ATT CGG CAC CAA AAA GCT; *dALS*-R, AGA TTG GCG AAC GGC AAG T; *IMP-L2*-F, CAC TGG CTC CAA GAC CAT CT; *IMP-L2*-R, AGG TAT CGG CGG TAT CCT TT; *GAPDH2*-F, GCG GTA GAA TGG GGT GAG AC; *GAPDH2*-R, TGA AGA GCG AAA ACA GTA GC.

Fecundity Assay. For each genotype (GC-less *y w*/*y w*; UASp-*bam*$^{+}$/+; *nos*-GAL4::VP16/+; and fertile *y w*/*y w*; UASp-*bam*$^{+}$/+), we measured fecundity using 10 single adult (1-day-old) females kept with 2 *y w* males in vials containing standard fly food medium with live yeast sprinkled on top. Flies were passed daily to new vials, and fecundity was measured over 10 days posteclosion.

Carbohydrate Measurements. To measure circulating carbohydrates (glucose plus trehalose), hemolymph samples were collected from 10-day-old females by decapitating the heads. For each genotype, we collected a total of 0.3 μl of hemolymph by extracting ≈20–30 flies; hemolymph samples and standards were added to 75 μl of Infinity Glucose Reagent (ThermoElectron) in 96-well plates. To determine stored glucose (whole-body glucose), we homogenized flies in 1 ml of ice-cold homogenization buffer [0.01M KH_2PO_4, 1 mM EDTA, pH 7.4, plus protease inhibitors (CompleteMini, Roche)] and used 25 μl of homogenate to measure glucose with the Infinity Glucose Reagent. Total glucose was measured by reading absorbance at 340 nm after 3 min of incubation at 37°C. To measure trehalose in the samples, porcine kidney trehalose (Sigma Chemical, T8778) at 5 μl per 5 ml was added, the solution returned to 37°C overnight, followed by a second reading of absorbance at 340 nm. The amount of trehalose was calculated from the second absorbance reading minus that of the first reading.

DILP Immunocytochemistry. For DILP immunocytochemistry, brains of 10-day-old adult females were dissected into PBS, fixed for 1 h with fresh 4% paraformaldehyde, washed in PBS three times for 5 min, washed in PBT (PBS with 0.3% Triton X-100) three times for 20 min, and then blocked in PBT plus 1% BSA three times for 20 min at room temperature. Brains then were incubated overnight in 1:1,000 primary DILP antibody in PBT (polyclonal anti-rabbit antibody against A chain of *D. melanogaster* DILP; 440D antiserum; courtesy of M. Brown, University of Georgia) (1) at 4°C. The next day, samples were washed in PBT three times for 20 min and incubated for 2 h in 1:500 secondary antibody (Alexa Fluor 594-conjugated goat anti-rabbit IgG; Molecular Probes) in PBT at room temperature. After incubation in secondary antibody, brains were washed in PBT three times for 20 min, followed by three 5-min washes in PBS, and mounted in ProLong Gold mounting medium (Invitrogen). Images were processed using a Zeiss AxioVision Z1 fluorescent microscope with ApoTome optics (Zeiss) and Zeiss AxioVision software suite (version 4.5). The IPCs in Fig. S4*A* were visualized by overexpressing GFP under the control of a *dilp2*-GAL4 driver (*dilp2*-GAL4; UAS-*CD8*::*gfp*) (2).

FOXO Immunocytochemistry. As described in ref. 3, whole-mount samples of peripheral fat body tissue from the posterior abdomen of 10-day-old adult females were dissected into PBS, fixed in fresh 4% paraformaldehyde, incubated in anti-dFOXO (1:500, guinea pig antiserum; courtesy of H. Broihier, Case Western Reserve University), followed by incubation in Alexa Fluor 568-conjugated secondary antibody (1:2,000; Molecular Probes), and then mounted in ProLong Gold mounting medium with DAPI (Invitrogen). Samples were visualized and images processed using a Zeiss Axioplan 2 fluorescent microscope and Zeiss AxioVision software (version 4.5).

FOXO Western Blot Analysis. For each genotype, we generated lysates from 160 decapitated bodies from 10-day-old females. Cytoplasmic and nuclear extracts were prepared from lysed tissues by using the Nuclear Extract Kit (Active Motif, #40010), and protein concentration was determined with the BCA Protein Assay Kit (Pierce), following the manufacturers' protocols. For Western blot analysis, we loaded 10 μg of protein per lane using a NuPAGE 4–12% Bis-Tris Gel (Invitrogen). Antibodies used were guinea pig anti-dFOXO (a gift from H. Broihier, Case Western Reserve University), mouse anti-Lamin DMO (ADL84.12, Developmental Studies Hybridoma Bank, University of Iowa) as nuclear control, and rabbit anti-Hsp90 (SPA-846, Stressgen) as a cytoplasmic control. The intensity of each band was analyzed by using Image J software (http://rsb.info.nih.gov/ij/). For intensity analysis, the amount of dFOXO protein was corrected for nuclear contamination of the cytoplasmic fraction by quantifying and subtracting the amount of Lamin protein found in the cytoplasmic fraction.

1. Cao C, Brown MR (2001) Localization of an insulin-like peptide in brains of two flies. *Cell Tiss Res* 304:317–321.
2. Ikeya T, Galic M, Belawat P, Nairz K, Hafen E (2002) Nutrient-dependent expression of insulin-like peptides from neuroendocrine cells in the CNS contributes to growth regulation in *Drosophila Curr Biol* 12:1293–1300.
3. Hwangbo DS, Gersham B, Tu M-P, Palmer M, Tatar M (2004) *Drosophila* dFOXO controls lifespan and regulates insulin signalling in brain and fat body. *Nature* 429:562–566.
4. Broughton SJ, *et al* (2005) Longer lifespan, altered metabolism, and stress resistance in *Drosophila* from ablation of cells making insulin-like ligands. *Proc Natl Acad Sci USA* 102:3105–3110.
5. Brogiolo W, *et al* (2001) An evolutionarily conserved function of the *Drosophila* insulin receptor and insulin-like peptides in growth control. *Curr Biol* 11:213–221.
6. Rulifson EJ, Kim SK, Nusse R (2002) Ablation of insulin-producing neurons in flies: Growth and diabetic phenotypes. *Science* 296:1118–1120.

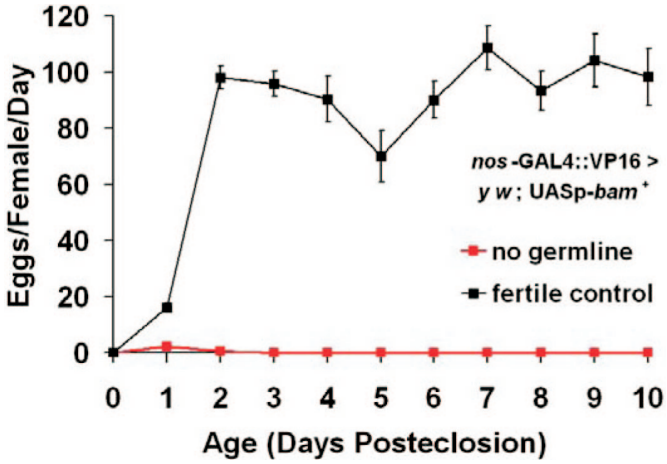

Fig. S1. GC loss causes female sterility. Early fecundity over the first 10 days posteclosion in females ectopically misexpressing *bam*$^{+}$ in the germ line (no germ line: *y w*/*y w*; UASp-*bam*$^{+}$/+; *nos*-GAL4::VP16/+) relative to a fertile control (*y w*/*y w*; UASp-*bam*$^{+}$/+). GC loss in females misexpressing *bam*$^{+}$ causes sterility but occurs after the ovary has completed its normal development. Females lay some eggs before they become fully sterile at around day 7 posteclosion. Also see Fig. 1.

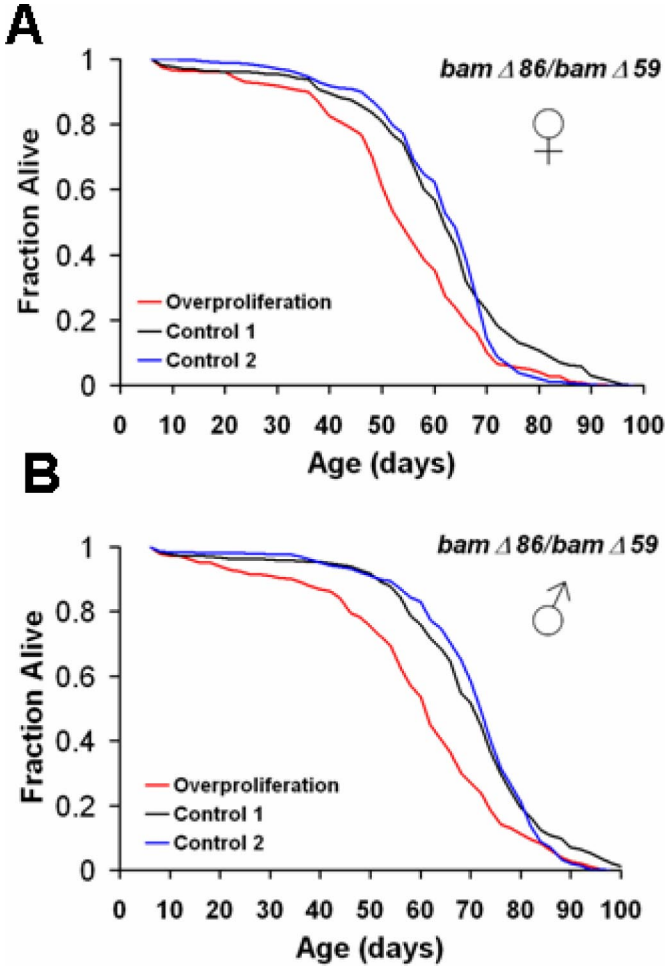

Fig. S2. GC overproliferation shortens lifespan. Survival is reduced in a heteroallelic *bam* null mutant (overproliferation: ry^{506} e^{1} $bam^{\Delta 86}$/*red e* $bam^{\Delta 59}$) compared with fertile controls (control 1: w^{1118}/+; ry^{506} e^{1} $bam^{\Delta 86}$; control 2: w^{1118}/+; *red e* $bam^{\Delta 59}$), among both females (*A*) and males (*B*). For survival statistics, see Table S1.

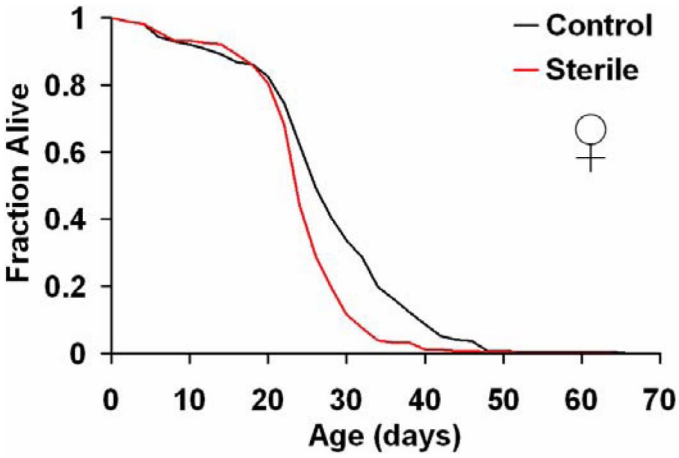

Fig. S3. Loss of oocytes is not sufficient for slowing aging. Lifespan is reduced in a female-sterile, heteroallelic mutant genotype of *egl* (sterile: *w*; *cn bw* egl^{PR29}/*cn bw* egl^{wu50}) compared with a fertile control carrying a transgenic rescue construct [control: *w*; *cn bw* egl^{PR29}/*cn bw* egl^{wu50}; *CA8B*(egl^{+})/+]. See Table S1 for survival statistics.

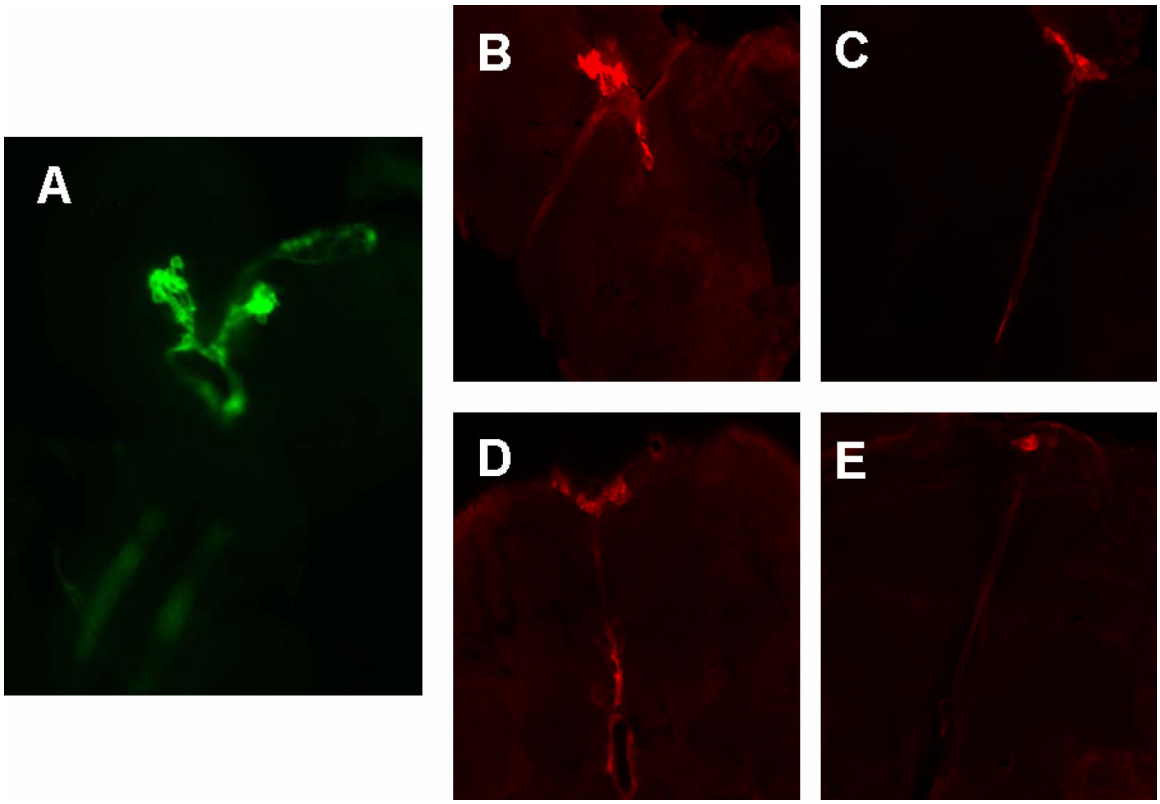

Fig. S4. DILP immunostaining of IPCs and axonal projections. (*A*) The pars intercerebralis of the fly brain contains the major insulin-producing cells (IPCs; in green, with GFP), which are functionally equivalent to the mammalian pancreatic β cells (2, 4–6). The IPCs form two bilaterally paired clusters of seven median neurosecretory cells (mNSCs), which contact the heart via axonal projections and release DILPs into the circulatory system to homeostatically regulate circulating sugar levels (4–6). The image shows the IPCs in the brain of a 10-day-old adult female fly overexpressing a GFP construct, driven with a *dilp2*-GAL4 line (*dilp2*-GAL4; UAS-*CD8*::*gfp*). (*B* and *C*) IPCs in GC-less (*y w*/*w*^{1118}; UASp-*bam*$^{+}$::*gfp*/+; *nos*-GAL4::VP16/+) flies. (*D* and *E*) IPCs in fertile control flies (*y w*/*y w*; UASp-*bam*$^{+}$::*gfp*/+). DILP protein in IPCs and their axonal projections was visualized with antiserum against DILP in 10-day-old adult females; shown are IPCs from two different individuals for each genotype. Qualitative inspection of *z* stack projections ($n = 15$ for each genotype; exposure time: 14 s) suggests that brains of GC-less flies produce as much and, in some cases, more DILP protein in the cell bodies of the IPCs than in fertile controls. Strong axonal staining is indicative of functional transport of DILP vesicles along the axon.

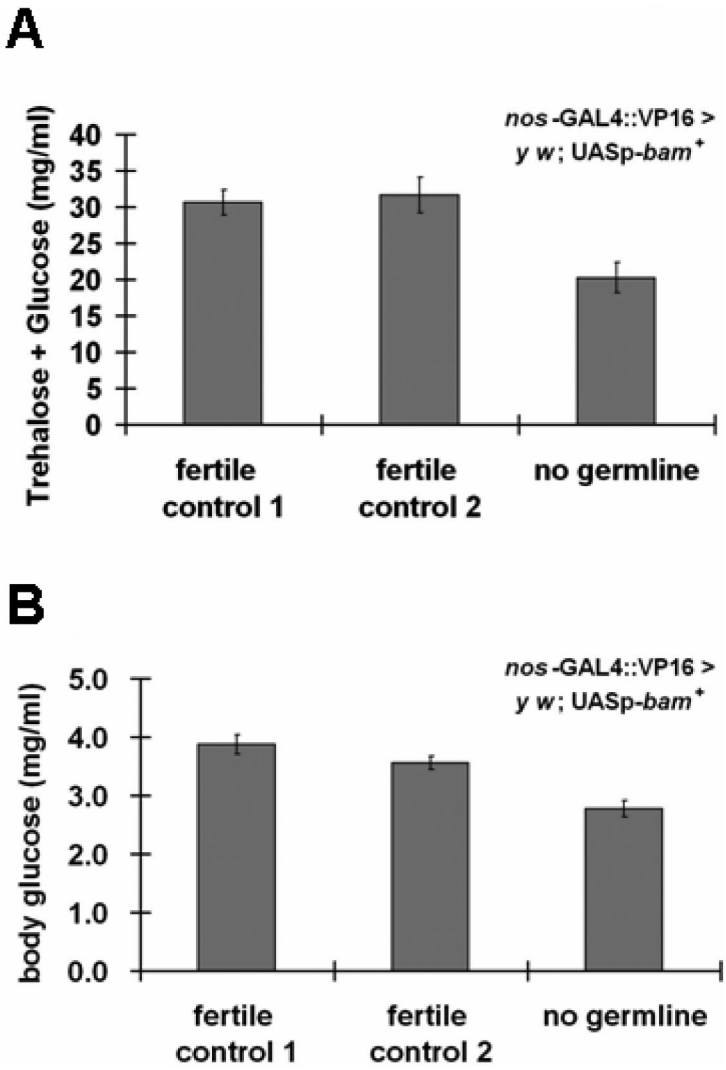

Fig. S5. GC loss lowers carbohydrate levels. In the fly hemolymph, circulating carbohydrates consist of trehalose (a glucose disaccharide) and glucose (free, monomeric glucose); together these sugars represent the combined total pool of hemolymph glucose (4, 6). (*A* and *B*) GC-less flies (*y w*/*w*^{1118}; UASp-*bam*$^{+}$::*gfp*/+; *nos*-GAL4::VP16/+) have lowered circulating levels of hemolymph glucose (glucose plus trehalose) (*A*) and exhibit a reduction in total stored glucose levels compared with fertile control flies (*y w*/*y w*; UASp-*bam*$^{+}$::*gfp*/+) (*B*). Because IPC-produced DILPs tightly regulate sugar levels in the fly (4, 6), these data suggest that increased neural DILP production in GC-less flies causes reduction in carbohydrate levels.

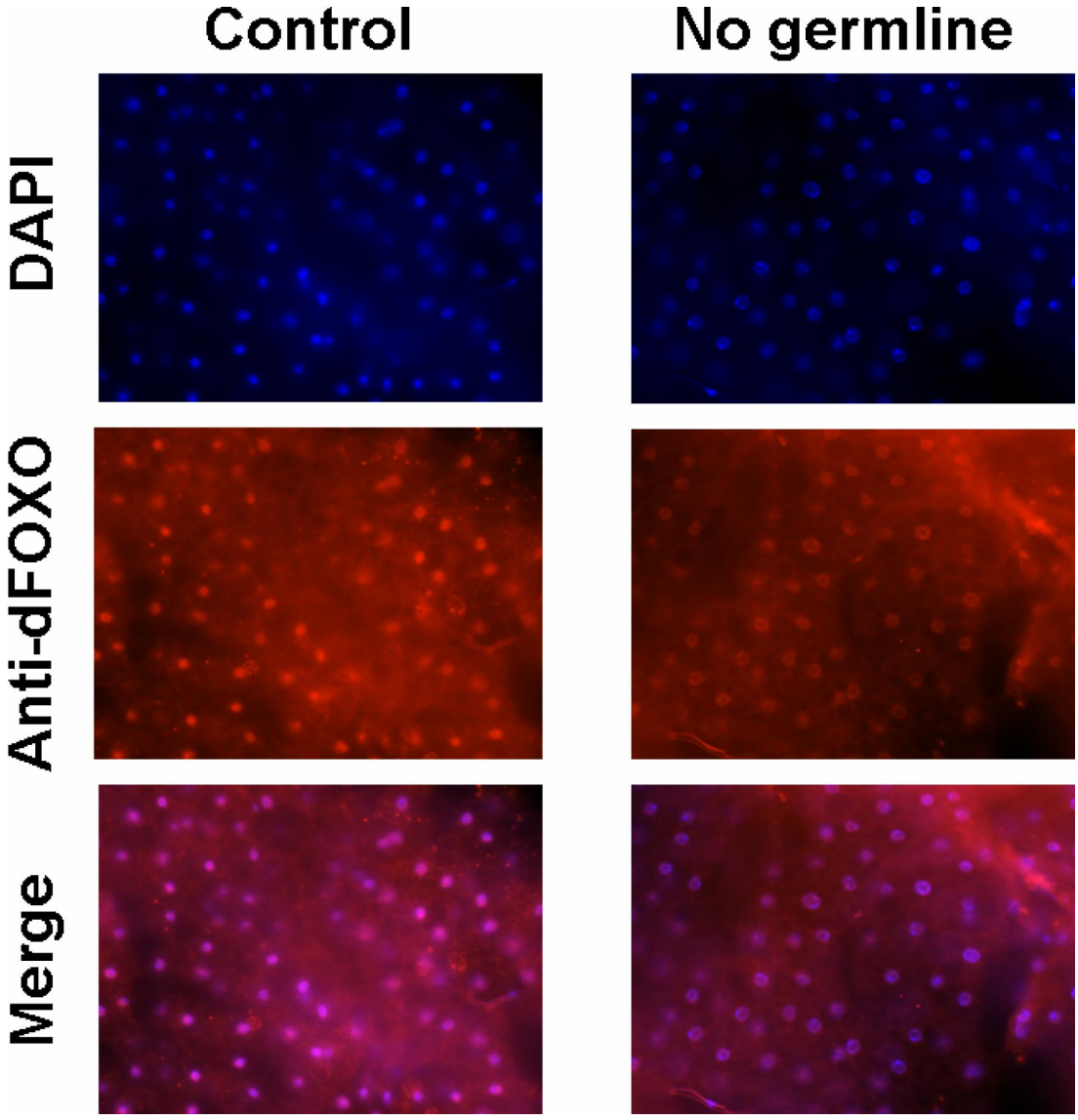

Fig. S6. Effects of GC loss on dFOXO localization in fat body. Reduced IIS can cause nuclear localization of dFOXO in target tissues, and subcellular localization of dFOXO can be used as a proxy for IIS activity (3). Peripheral fat body tissue (whole-mount tissue) of 10-day-old females was stained with anti-dFOXO antibody. In both fertile control flies (left lane; *y w*/*y w*; UASp-*bam*$^{+}$::*gfp*/+) and GC-less flies (right lane; *y w*/*w*^{1118}; UASp-*bam*$^{+}$::*gfp*/+; *nos*-GAL4::VP16/+), most fat body cell nuclei are dFOXO^{+}, suggesting that dFOXO is mainly nuclear (blue, DAPI, nuclear counterstain; red, anti-dFOXO; purple, merge), which suggests that dFOXO might be active in both GC-less and control flies (also see Fig. S7).

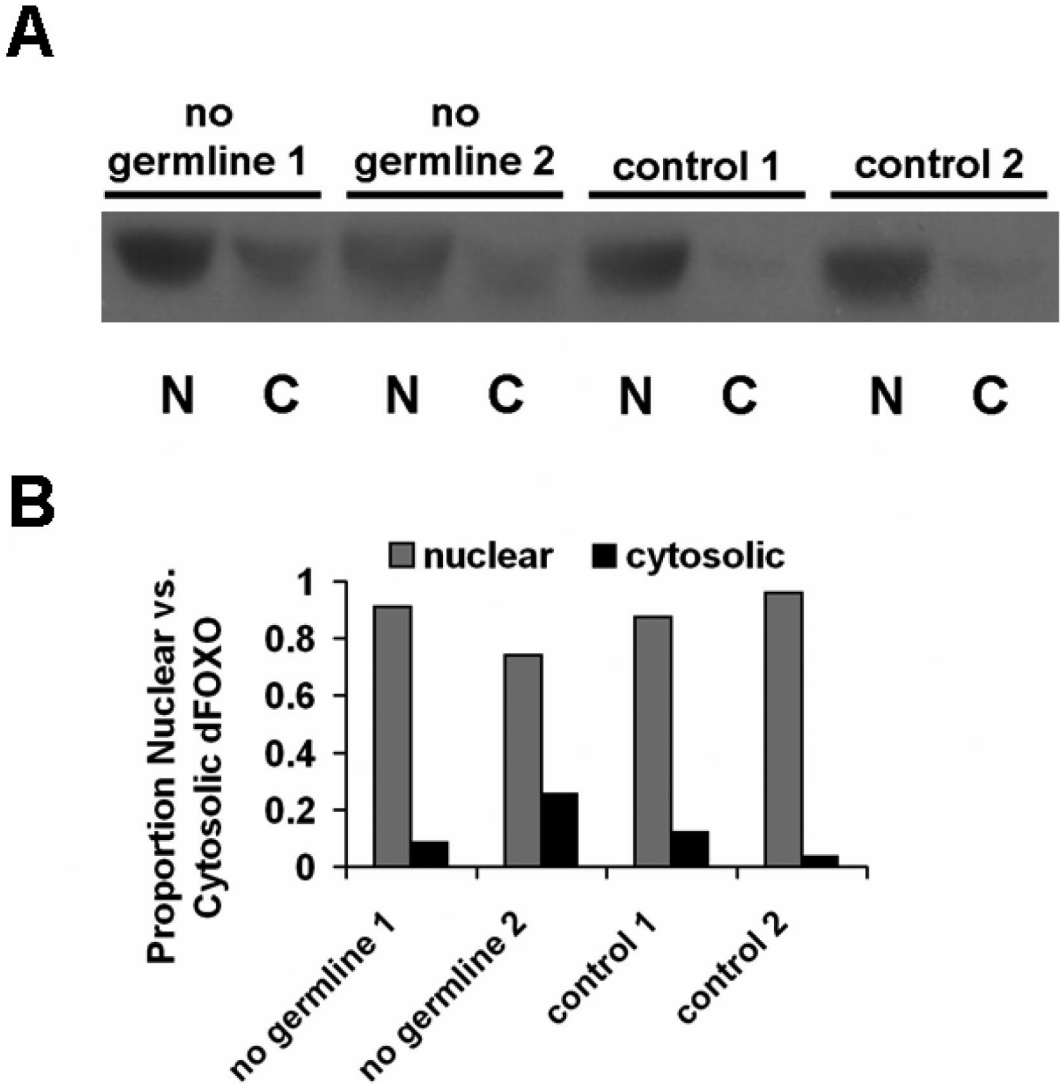

Fig. S7. Subcellular localization of dFOXO in whole-body tissue. (*A*) Western blot analysis with anti-dFOXO antibody, performed on nuclear (N) and cytosolic (C) fractions of whole bodies (without heads) of 10-day-old females. GC-less genotypes 1 and 2 have identical genotype (*y w*/*w*^{1118}; UASp-*bam*$^{+}$::*gfp*/+; *nos*-GAL4::VP16/+); however, as an internal control, crosses were set up in two ways: (*i*) by crossing UAS females to GAL4 males and (*ii*) reciprocally, by crossing GAL4 females to UAS males. Control 1 flies are *y w*/*y w*; UASp-*bam*$^{+}$::*gfp*/+; control 2 flies are *y w*/*w*^{1118}; *nos*-GAL4::VP16/+. In both GC-less and control flies, dFOXO is predominantly nuclear. (*B*) Quantification of band intensity of the Western blot shown in *A*. dFOXO is mainly nuclear, both in GC-less and control flies, suggesting that the nuclear localization pattern of dFOXO does not differ between flies with and without GC loss. Despite the lack of a difference in the nuclear localization pattern among genotypes, GC-less flies show strong up-regulation of transcriptional targets of dFOXO (Fig. 3).

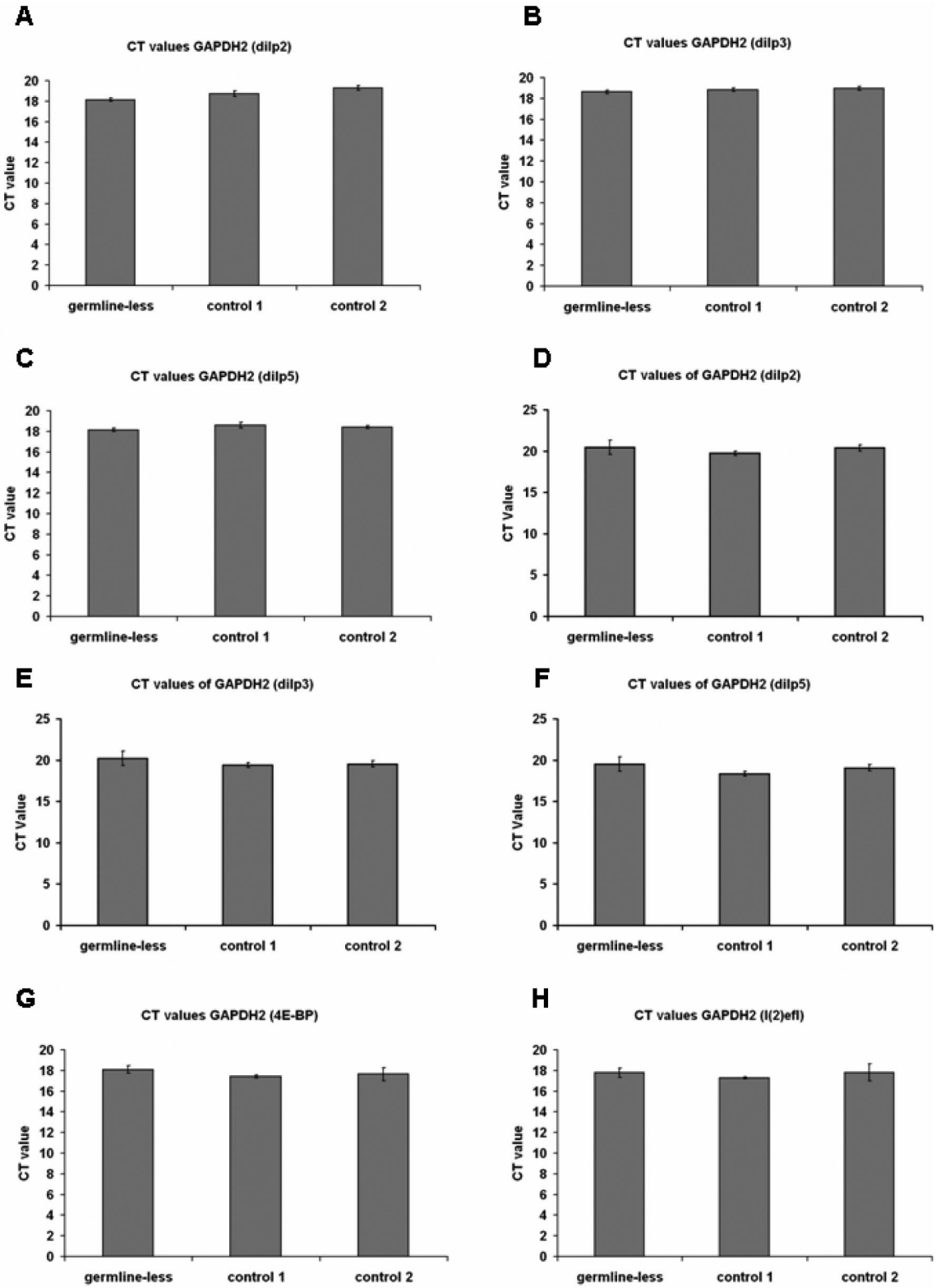

Fig. S8. CT values of GAPDH2 controls used in qPCR experiments shown in Fig. 3. (*A–H*) CT values for the GAPDH2 normalization control do not differ among GC-less flies and control genotypes 1 and 2 (one-way ANOVA with factor ''genotype'': $F_{(2,9)} > 0.29$, $P > 0.05$, in all experiments), which suggests that differences in mRNA transcript levels between flies with and without GC loss are not confounded by changes in the normalization control.

Table S1. Statistical analysis of lifespan

Genotype	Sex	Fig.	Treatment	*N*(0)	Mean lifespan	SE	Median lifespan	χ^2	*P*	Percentage change
y w/w^{1118};UASp-bam^{+}::gfp/+; nos-GAL4::VP16/+	F	2*A*	No germ line	285	40.8	0.60	42	—	—	—
y w/y w;UASp-*bam^{+}::gfp/+*	F	2*A*	Control 1	303	30.9	0.53	32	189.3	<0.0001	**31.3**
y w/w^{1118}; nos-GAL4::VP16/+	F	2*A*	Control 2	306	29.4	0.64	28	169.0	<0.0001	**50.0**
y w/w^{1118};UASp-bam^{+}::gfp/+; nos-GAL4::VP16/+	M	2*B*	No germ line	278	45.8	0.61	46	—	—	—
y w/y w;UASp-*bam^{+}::gfp/+*	M	2*B*	Control 1	237	37.1	0.78	38	67.7	<0.0001	**21.0**
y w/w^{1118}; nos-GAL4::VP16/+	M	2*B*	Control 2	290	36.4	0.77	36	67.1	<0.0001	**27.8**
w^{1118}/w^{1118};UASp-bam^{+}::gfp/+; nos-GAL4::VP16/*bam$^{\Delta 86}$*	F	2*C*	No germ line	240	40.2	0.63	42	—	—	—
w^{1118}/w^{1118};UASp-bam^{+}::gfp/+; bam$^{\Delta 86}$/+	F	2*C*	Control 1	249	32.5	0.64	32	60.2	<0.0001	**31.3**
w^{1118}/w^{1118}; nos-GAL4::VP16/+	F	2*C*	Control 2	247	35.6	0.65	34	17.7	<0.0001	**23.5**
w^{1118}/w^{1118};UASp-bam^{+}::gfp/+; nos-GAL4::VP16/*bam$^{\Delta 86}$*	M	2*D*	No germ line	312	46.8	0.82	48	—	—	—
w^{1118}/w^{1118};UASp-bam^{+}::gfp/+; bam$^{\Delta 86}$/+	M	2*D*	Control 1	300	34.0	0.72	30	130.2	<0.0001	**60.0**
w^{1118}/w^{1118}; nos-GAL4::VP16/+	M	2*D*	Control 2	323	40.4	0.72	36	29.9	<0.0001	**33.3**
y w/y^{1} w;*UASp-*bam^{+}::gfp/NGT*-GAL4,	F	2*E*	No germ line	315	63.5	0.84	66	—	—	—
y w/y w;UASp-*bam^{+}::gfp/+*	F	2*E*	Control 1	303	30.9	0.53	32	609.7	<0.0001	**100.1**
y w/y^{1} w; NGT*-GAL4	F	2*E*	Control 2	291	47.5	0.87	46	186.0	<0.0001	**43.5**
y w/y^{1} w;*UASp-*bam^{+}::gfp/NGT*-GAL4,	M	2*F*	No germ line	230	64.1	0.87	68	—	—	—
y w/y w;UASp-*bam^{+}::gfp/+*	M	2*F*	Control 1	237	37.1	0.78	38	403.5	<0.0001	**78.8**
y w/y^{1} w; NGT*-GAL4	M	2*F*	Control 2	252	53.9	0.88	56	79.3	<0.0001	**21.4**
w^{1118}/y^{1} w;*UASp-*bam^{+}::gfp/NGT*-GAL4; *bam$^{\Delta 86}$/+*	F	2*G*	No germ line	315	57.1	0.81	62	—	—	—
w^{1118}/y w;UASp-bam^{+}::gfp/+; bam$^{\Delta 86}$/+	F	2*G*	Control 1	360	47.9	0.68	48	99.4	<0.0001	**29.2**
y w/y^{1} w; NGT*-GAL4/+	F	2*G*	Control 2	354	45.0	0.58	44	225.8	<0.0001	**41.0**
w^{1118}/y^{1} w;*UASp-*bam^{+}::gfp/NGT*-GAL4; *bam$^{\Delta 86}$/+*	M	2*H*	No germ line	308	60.0	0.87	64	—	—	—
w^{1118}/y w;UASp-bam^{+}::gfp/+; bam$^{\Delta 86}$/+	M	2*H*	Control 1	337	55.5	0.75	56	18.9	<0.0001	**14.3**
y w/y^{1} w; NGT*-GAL4/+	M	2*H*	Control 2	348	50.7	0.61	52	157.8	<0.0001	**23.1**
ry^{506} e^{1} bam$^{\Delta 86}$/red e bam$^{\Delta 59}$	F	S2*A*	Overproliferation	434	51.1	0.92	54	—	—	—
w^{1118}/+; ry^{506} e^{1} bam$^{\Delta 86}$	F	S2*A*	Control 1	447	61.1	0.60	64	40.1	<0.0001	*−15.6*
w^{1118}/+; red e bam$^{\Delta 59}$/+	F	S2*A*	Control 2	406	61.2	0.83	62	60.49	<0.0001	*−13.0*
ry^{506} e^{1} bam$^{\Delta 86}$/red e bam$^{\Delta 59}$	M	S2*B*	Overproliferation	359	59.2	1.0	62	—	—	—
w^{1118}/+; ry^{506} e^{1} bam$^{\Delta 86}$	M	S2*B*	Control 1	432	68.9	0.83	72	40.8	<0.0001	*−13.9*
w^{1118}/+; red e bam$^{\Delta 59}$/+	M	S2*B*	Control 2	368	68.4	0.96	72	46.2	<0.0001	*−13.9*
w; cn bw egl^{PR29}/cn bw egl^{wu50}	F	S3	Sterile	445	31.1	0.52	32	—	—	—
w; cn bw egl^{PR29}/cn bw egl^{wu50}; CA8B(*egl^{+}*)/+	F	S3	Control	446	35.7	0.62	34	56.9	<0.0001	*−5.9*

Results grouped by experiment and sex (F, female; M, male). Reported are initial cohort size [*N*(0)]; mean lifespan, standard error (SE), and median lifespan in days; χ^2 test statistic and *P* value from log-rank test; and percentage change in median lifespan of experimental treatment relative to each control. We performed pairwise comparisons between treatment (e.g., ″no germ line″) and each control with log-rank tests. Significant increases in median lifespan relative to control are indicated in bold, and significant decreases relative to control are in italics.